Neuronal, stromal, and T-regulatory cell crosstalk in murine skeletal muscle

Kathy Wang[a,b,1,2], Omar K. Yaghi[a,b,1], Raul German Spallanzani[a,b,1], Xin Chen[a,b,3], David Zemmour[a,b,4], Nicole Lai[a], Isaac M. Chiu[a], Christophe Benoist[a,b,5], and Diane Mathis[a,b,5]

[a]Department of Immunology, Harvard Medical School, Boston, MA 02115; and [b]Evergrande Center for Immunologic Diseases, Harvard Medical School and Brigham and Women's Hospital, Boston, MA 02115

Contributed by Diane Mathis, January 15, 2020 (sent for review December 23, 2019; reviewed by David A. Hafler and Jeffrey V. Ravetch)

A distinct population of Foxp3$^+$CD4$^+$ regulatory T (Treg) cells promotes repair of acutely or chronically injured skeletal muscle. The accumulation of these cells depends critically on interleukin (IL)-33 produced by local mesenchymal stromal cells (mSCs). An intriguing physical association among muscle nerves, IL-33$^+$ mSCs, and Tregs has been reported, and invites a deeper exploration of this cell triumvirate. Here we evidence a striking proximity between IL-33$^+$ muscle mSCs and both large-fiber nerve bundles and small-fiber sensory neurons; report that muscle mSCs transcribe an array of genes encoding neuropeptides, neuropeptide receptors, and other nerve-related proteins; define muscle mSC subtypes that express both IL-33 and the receptor for the calcitonin-gene–related peptide (CGRP); and demonstrate that up- or down-tuning of CGRP signals augments or diminishes, respectively, IL-33 production by muscle mSCs and later accumulation of muscle Tregs. Indeed, a single injection of CGRP induced much of the genetic program elicited in mSCs early after acute skeletal muscle injury. These findings highlight neural/stromal/immune-cell crosstalk in tissue repair, suggesting future therapeutic approaches.

muscle repair | regulatory T cells | stromal cells | CGRP | IL-33

Crosstalk between the immune system and the sensory nervous system, both of which rapidly respond to damaging and painful stimuli, has become increasingly apparent over the past several years (1). For example, targeted ablation of nociceptive sensory neurons in the respiratory tract reduces allergic airway inflammation (2), skin nociceptors drive psoriasis via stimulation of dendritic cells (3), nociceptors modulate immune responses against bacterial and fungal pathogens (4, 5), and activation of nociceptors in a mouse model of inflammatory bowel disease exacerbates colonic inflammation via release of substance P (6).

Recent studies have uncovered a potential role for nervous:immune system interactions, channeled through stromal cell production of interleukin (IL)-33, in skeletal muscle regeneration (7). IL-33, an alarmin of the IL-1 family of inflammatory cytokines, is constitutively expressed in the nucleus until it is released from the cell subsequent to necrotic death, mechanical injury, or other types of stress in order to alert the immune system to tissue damage (8). While this cytokine was originally investigated primarily as a stimulator of type 2 immunity, in particular, allergic inflammation, more recent reports have highlighted its function in driving the accumulation of Foxp3$^+$CD4$^+$ regulatory T (Treg) cell populations operating in nonlymphoid tissues; notably the colon, visceral adipose tissue, and skeletal muscle (7, 9–12). Muscle Tregs express high levels of the IL-33 receptor, ST2 (encoded by *Il1rl1*), and loss- and gain-of-function experiments have demonstrated the importance of both muscle Tregs and their expression of ST2 for optimal regeneration after acute injury (7, 13).

The primary IL-33–producing cells in mouse skeletal muscle are mesenchymal stromal cells (mSCs), included within a fraction displaying the markers Sca-1 and PDGFRα, but not the hematopoietic and endothelial cell markers, CD45 and CD31, respectively (7). This fraction of muscle mSCs (MmSCs) has repeatedly been implicated in healthy tissue repair (14, 15). MmSC expression of IL-33 is boosted on acute injury, and is reduced in aged mice characterized by poor muscle regeneration (7). IL-33$^+$ mSCs can be found in close association with nerve structures in skeletal muscle, including nerve fibers, nerve bundles, and muscle spindles that control proprioception (7).

Given the intriguing functional and/or physical associations among muscle nerves, mSCs, and Tregs, and in particular, their co-ties to IL-33, we were inspired to more deeply explore this axis. Here, we used whole-mount immunohistochemical imaging as well as population-level and single-cell RNA sequencing (scRNA-seq) to examine the neuron/mSC/Treg triumvirate in hindlimb muscles. We identified a set of MmSC transcripts encoding neural signaling molecules; notably, both subunits of the receptor for the sensory neuropeptide, calcitonin gene-related peptide (CGRP). In vivo pharmacological or genetic manipulations of CGRP signaling modulated IL-33 expression by mSCs and the accumulation of Tregs, pointing to functionally relevant tricellular crosstalk.

Significance

A distinct population of Foxp3$^+$CD4$^+$ regulatory T (Treg) cells promotes repair of injured skeletal muscle. In mice, accumulation of these cells depends on interleukin (IL)-33 produced by local stromal cells. We demonstrate a striking proximity between IL-33$^+$ muscle mSCs and both large-fiber nerve bundles and small-fiber sensory neurons. Muscle stromal cells transcribe an array of genes encoding neuropeptides, neuropeptide receptors, and other nerve-related proteins; in particular, one subtype expresses both IL-33 and the receptor for the calcitonin-gene–related peptide (CGRP). Up- or down-tuning of CGRP signals augments or diminishes, respectively, IL-33 production by muscle mSCs and accumulation of muscle Tregs. These findings highlight neural/stromal/immune-cell crosstalk in tissue repair, suggesting future therapeutic approaches.

Author contributions: K.W., O.K.Y., R.G.S., X.C., C.B., and D.M. designed research; K.W., O.K.Y., R.G.S., and X.C. performed research; N.L. and I.M.C. contributed new reagents/analytic tools; K.W., O.K.Y., R.G.S., D.Z., and D.M. analyzed data; and K.W., O.K.Y., R.G.S., and D.M. wrote the paper.

Reviewers: D.A.H., Yale University School of Medicine; and J.V.R., Rockefeller University.

The authors declare no competing interest.

Data deposition: The data reported in this paper have been deposited in the Gene Expression Omnibus (GEO) database, https://www.ncbi.nlm.nih.gov/geo/ (accession no. GSE143428).

[1]K.W., O.K.Y., and R.G.S. contributed equally to this work.

[2]Present address: Department of Surgery, University of Illinois - Chicago Metropolitan Group Hospitals, Chicago, IL 60657.

[3]Present address: BeiGene, Beijing City, China 102206.

[4]Present address: Department of Pathology, Brigham and Women's Hospital, Boston, MA 02115.

[5]To whom correspondence may be addressed. Email: cbdm@hms.harvard.edu.

This article contains supporting information online at https://www.pnas.org/lookup/suppl/doi:10.1073/pnas.1922559117/-/DCSupplemental.

Results

Visualization of Skeletal Muscle Neurons and Tregs in Relation to IL-33–Expressing Stromal Cells. The acute muscle injury provoked by injection of cardiotoxin (CTX) is accompanied by an expansion of the local Treg population, typically peaking at 3 to 4 d postinjection (13). There is also a rapid increase in the local expression of IL-33 and an enrichment in IL-33$^+$ mSCs (7). We examined the proximity of muscle Tregs and IL-33$^+$ mSCs via fluorescent anti–IL-33 antibody (Ab) staining of hindlimb muscle 3 d after CTX-induced injury of B6.*Foxp3-IRES-GFP* reporter mice. Low-power magnification revealed clusters of Foxp3$^+$ cells intermingled with conglomerates of IL-33$^+$ cells (Fig. 1 *A*, *Left*), while higher magnification demonstrated close association and occasional overlap between the two cell types (Fig. 1 *A*, *Middle* and *Right*).

We previously reported that IL-33$^+$ cells are often associated with neural structures in skeletal muscle, including large-diameter NF200$^+$ nerve bundles, nerve fibers, and muscle spindles (7). In

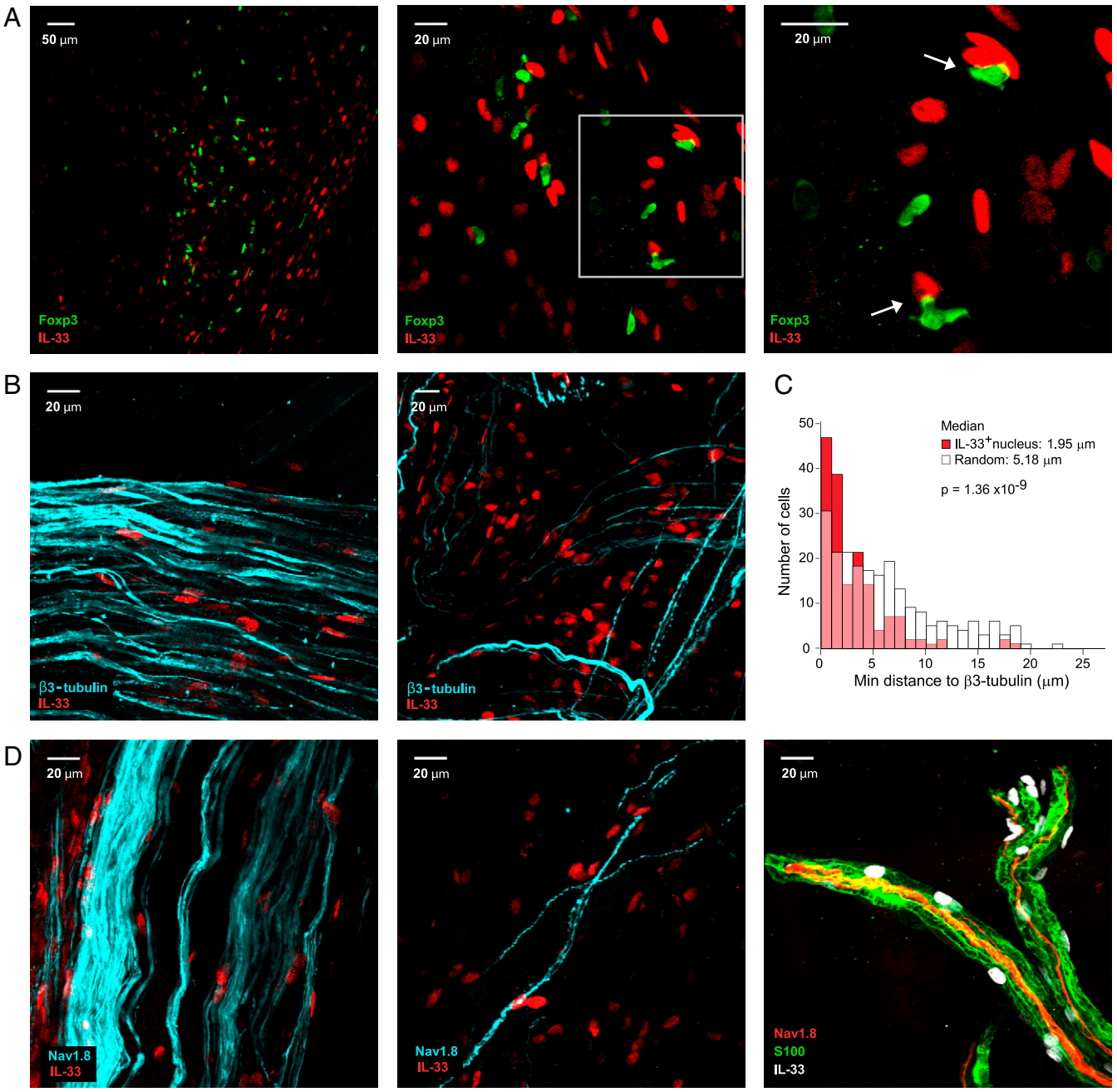

Fig. 1. Association among Tregs, IL-33$^+$ cells, and peripheral nerves within mouse skeletal muscle. Immunofluorescence imaging of whole-mount tissue from hindlimb muscle. (*A*) Tregs and IL-33$^+$ cells, 3 d post-CTX injury, at 10× magnification (*Left*), 60× (*Middle*), and 130× (*Right*). White arrows: Tregs and IL-33$^+$ cells within contact distance. (*B*) Colocalization of IL-33$^+$ cells with β3-tubulin$^+$ nerve fibers in uninjured muscle (*Left*) and 3 d post-CTX injury (*Right*). (*C*) Minimum distances from either the centers of IL-33$^+$ cells or random points to β3-tubulin$^+$ area in uninjured muscle. Plotted as kernel density distribution from composite of four images. *P* value determined by Kolmogorov–Smirnov test. (*D*) Colocalization of IL-33$^+$ cells with Nav1.8$^+$ nerve fibers in uninjured muscle (*Left*), 3 d post-CTX injury (*Middle*), and 12 h post-CTX injury with additional staining of S100$^+$ myelin sheath (*Right*). Pseudocoloring used for better visualization.

order to refine these initial observations, we first stained hindlimb muscle for IL-33 and for a universal marker of neural structures, the neuron-specific microtubule, β3-tubulin. A close association between cells expressing the two indicators was observed in both uninjured (Fig. 1 *B*, *Left*) and injured (Fig. 1 *B*, *Right*) muscle. Quantitative analysis of the minimum distance between β3-tubulin$^+$ axons and IL-33$^+$ stromal cells showed statistically greater proximity in comparison with that between β3-tubulin$^+$ axons and random points (Fig. 1*C*). Based on a broad assessment of all acquired images (including staining for additional markers), IL-33–expressing cells were almost always associated with nerves within hindlimb muscle, with >80% of IL-33$^+$ stroma lying close to β3-tubulin$^+$ nerves. However, IL-33 expressers were less frequently associated with unmyelinated single nerve fibers than with larger nerves and axon bundles, with only ∼20% of IL-33$^+$ cells visualized adjacent to thin nerve fibers.

Next, we determined whether IL-33$^+$ cells were associated with peripheral sensory neurons in particular, using B6.*Nav1.8-TdTomato* reporter mice. Neurons expressing the voltage-gated sodium channel Nav1.8 encompass 75% of the cell bodies in the dorsal root ganglia (which hold the sensory neuron afferents), marking mostly unmyelinated c-fibers, of which a large subset are nociceptors responsible for transmitting mechanical, cold, and inflammatory pain (reviewed in ref. 16). IL-33$^+$ nuclei were found in close proximity to Nav1.8$^+$(TdTomato) fibers in both uninjured and injured muscle (Fig. 1 *D*, *Left* and *Middle*). Covisualizing IL-33, Nav1.8, and S100 (which marks the myelin sheath) also revealed an intimate association between IL-33$^+$ cells and branching sensory axons (Fig. 1 *D*, *Right*).

The Transcriptome of MmSCs Revealed a Potential for Neuronal Interactions. In order to identify pathways and molecules that might be involved in interactions between neural and stromal cells, as suggested by their proximity, we performed population-level RNA-seq analysis of mSCs, the primary IL-33 expressors in skeletal muscle (7). Hindlimb muscles from uninjured 8-wk-old C57BL/6 (B6) males were removed, single-cell suspensions prepared, and mSCs double-sorted as CD45$^-$CD31$^-$Sca-1$^+$PDGFRα$^+$. The analogous lymph-node population was isolated from the same mice to serve as a comparator.

Several genes encoding neuropeptides, neuropeptide receptors, or other nerve-related proteins were expressed by mSCs from muscle and LNs, certain of them preferentially by the former tissue (Fig. 2 and *SI Appendix*, Fig. S1). The neuropeptide gene transcripts included *Penk*, which encodes the endogenous opioid proenkephalin, the precursor of met- and leu-enkephalins; *Dbi*, specifying a GABA receptor modulator; and *Nucb2*, which encodes Nesfatin-1, an appetite regulator (Fig. 2*A* and *SI Appendix*, Fig. S1*A*). Neuropeptide receptor gene transcripts included those encoding natriuretic peptide receptors (*Npr1*, *Npr2*), and *Adipor1*, specifying the Adiponectin receptor (Fig. 2*B* and *SI Appendix*, Fig. S1*B*). Other nerve-related genes expressed by mSCs encoded neurotrophic factors that promote neuronal survival (*Serpinf1*, *Ntrk2*, and *Nenf*); molecules involved in axon guidance (*Sema3c*, *Sema5a*, *Ntn1*, *Spon1*, and *Rgmb*); the enzyme monoamine oxidase B (*Maob*), which degrades neuroactive amines; and the muscle-specific receptor tyrosine kinase that regulates formation of neuromuscular junctions (*Musk*; Fig. 2*C* and *SI Appendix*, Fig. S1*C*).

Our attention was drawn in particular to transcripts encoding the calcitonin receptor-like receptor (CALCRL) and the receptor activity-modifying protein (RAMP)1, which combine to form the CGRP receptor, which is interesting from several perspectives. First, CALCRL is a G protein-coupled receptor, the ligand recognition of which depends on which RAMP subunit it associates with: combining CALCRL with RAMP1 yields the CGRP receptor, while its association with RAMP2 or RAMP3 produces the adrenomedullin receptor. The observation that transcripts encoding CALCRL and RAMP1 were both highly expressed in MmSCs suggests that the receptor complex might have a functional role in this tissue. Second, CGRP is involved in pain transmission and modulation throughout the central and peripheral nervous systems. This 37-amino acid peptide is released from peripheral sensory nerve terminals upon detection of damaging or proinflammatory signals via calcium influx into nerve terminals; for example, by triggering activation of the transient receptor potential vanilloid (TRPV)1 channel (reviewed in ref. 16). Upon release, it exerts a potent vasodilatory response within the microvasculature, thereby priming the inflammatory response. Many, though not all, CGRP$^+$ somatosensory neurons also express Nav1.8$^+$ (17). Last, while other cellular components of skeletal muscle tissue (endothelial, hematopoietic, or satellite cells) expressed detectable levels of *Ramp1* or *Calcrl* transcripts, mSCs were the only component that expressed high levels of both (*SI Appendix*, Table S1).

While population-level RNA-seq revealed that the MmSC compartment, specifically, the CD45$^-$CD31$^-$Sca-1$^+$PDGFRα$^+$

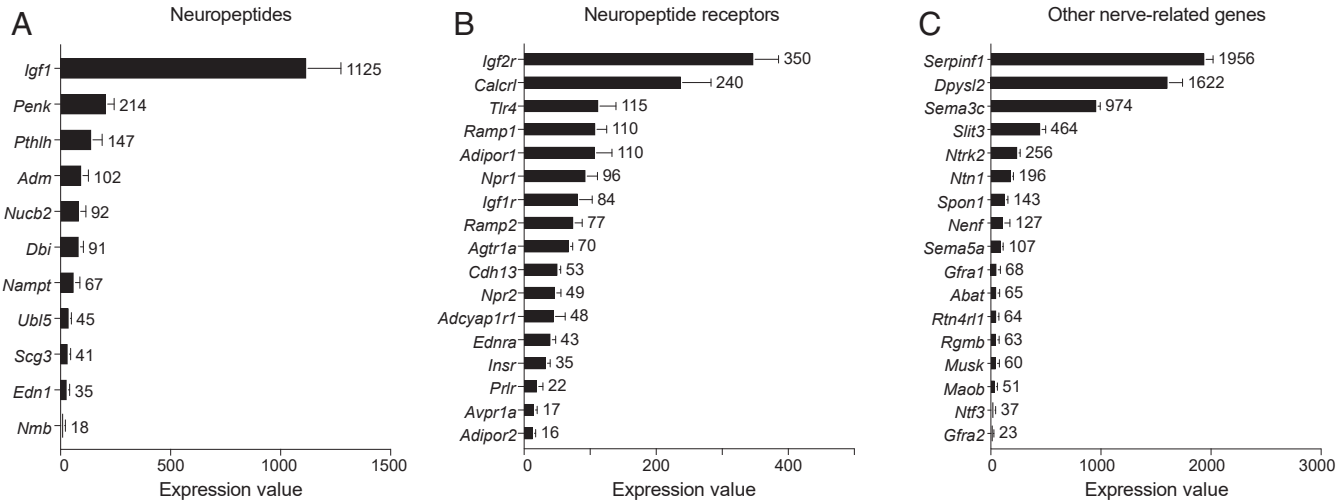

Fig. 2. MmSCs express genes involved in neural signaling. (*A*–*C*) RNA-seq analysis of mSCs isolated from uninjured hindlimb muscle. Triplicate samples. Average expression of select genes encoding neuropeptides (*A*), neuropeptide receptors (*B*), and other nerve-related genes involved in neurotrophic signaling, neuromodulation, and axon guidance (*C*).

component, expressed transcripts encoding IL-33, CALCRL, and RAMP-1, it was imperative to determine whether any MmSC subtype expressed all three transcripts, how frequent such cells were, and what transcriptional programs they evinced. Therefore, we carried out scRNA-seq analysis on mSCs sorted from uninjured hindlimb muscles of 8- to 10-wk-old B6 males. In total, 1,434 individual cells were measured; on average, 3,018 unique mRNA molecules transcribed from 1,408 different genes were sequenced per cell. We first displayed the combined data as a t-SNE (t-distributed Stochastic Neighbor Embedding) plot, permitting dimensionality reduction (Fig. 3*A*). Six distinct cell subtypes were discernible: MmSCs 1 through 6. As anticipated from the sorting strategy, all six subtypes expressed substantial levels of *Ly6a* (encoding Sca-1) and *Pdgfra*, evident from superimposing their transcript levels onto the t-SNE plot (Fig. 3*B*). However, *Il33*, *Calcrl*, and *Ramp1* all had more limited patterns of expression (Fig. 3*C*). Notably, MmSC1, and especially MmSC2 (which showed the highest expression of *Il33* transcripts), also expressed substantial levels of *Ramp1* and *Calcrl* transcripts.

To determine whether the CGRP receptor was present at the MmSC cell surface, we turned to flow cytometry, making use of a commercially available anti-RAMP1 Ab. An anti-CALCRL Ab was not available; however, RAMP1 would not be detectable at the surface unless bound to CALCRL. MmSCs from uninjured skeletal muscle did express RAMP1; hence, the CGRP receptor, at readily detectible levels (Fig. 3*D*). Gating MmSCs according to expression of CD26 permitted us to distinguish subtypes 1 and 2 ($CD26^{hi}$) from the other four subtypes ($CD26^{lo}$; Fig. 3*E*). Consistent with the scRNA-seq data, RAMP1 (hence the CGRP receptor) was displayed on MmSC subtypes 1 and 2 at elevated levels (Fig. 3*F*).

These findings prompted us to examine the localization of CGRP-expressing neurons vis-à-vis IL-33–expressing stromal cells. In uninjured hindlimb muscle, $IL\text{-}33^+$ cells were frequently observed adjacent to branching CGRP-immunoreactive sensory fibers at both low- and high-power magnification, highlighting their intimate association (Fig. 3*G*).

Manipulating CGRP Signals Impacted IL-33–Expressing mSCs and Tregs in Skeletal Muscle. To explore the functional relevance of CGRP, we performed both gain- and loss-of-function experiments. First, we intraperitoneally (i.p.) injected an optimized dose of CGRP into uninjured 7- to 9-wk-old B6 males and assessed IL-33 production in hindlimb tissue by an ELISA. A significant increase in the level of IL-33 was first evident at 4 h postinjection, which was further augmented at 8 h (Fig. 4*A*). At the latter time, there was also an increase in $IL\text{-}33^+$ mSCs in hindlimb muscle, assessed cytofluorimetrically (*SI Appendix*, Fig. S2*A* and Fig. 4*B*). Importantly, neither the viability of the MmSC compartment (*SI Appendix*, Fig. S2*B*) nor its relative contribution to the totality of muscle $IL\text{-}33^+$ cells (*SI Appendix*, Fig. S2*C*) changed during this time frame.

For deeper insights into the CGRP effects, we performed transcriptomic analyses on isolated MmSCs at the 4- and 8-h times. Three key findings emerged. First, volcano plots comparing injection of CGRP and PBS showed enrichment of G2M Checkpoint transcripts at 8 but not 4 h postinjection (Fig. 4*C*), in line with the increase in $IL\text{-}33^+$ MmSCs mentioned here. Second, KEGG pathway analysis highlighted a decrease (≤2-fold) in neuronal crosstalk at both 4 and 8 h and an increase (≥2-fold) in cytokine- and chemokine-related transcripts (*SI Appendix*, Table S2). Interestingly, the latter set of transcripts included those encoding the IL-33 receptor (*Il1rl1,* 27-fold), suggesting an IL-33-focused feedback or feed-forward loop. Finally, fold-change/fold-change plot revealed that much of the gene-expression program induced in hindlimb MmSCs on day 1 after CTX-induced muscle injury was also up-regulated by a single intraperitoneal injection of CGRP, although somewhat less so. In other words, most transcripts did not fall along the *x* or *y* axis in Fig. 4*D*, but rather along a diagonal.

Analysis of Tregs after repeated CGRP injection i.p. into uninjured 8- to 10-wk-old B6 males revealed the anticipated increase in their contribution to the $CD4^+$ T cell compartment in muscle but not spleen (Fig. 4*E*). This finding was solidified in a loss-of-function experiment. We compared uninjured 8-wk-old males deficient in $TRPV1^+$ nociceptor neurons or not (*Trpv1-Cre*$^{+/-}$/*Dta*$^{+/-}$ mice vs. *Trpv1-Cre*$^{-/-}$/*Dta*$^{+/-}$ littermates), and found that the $TRPV1^+$-neuron-deficient mice had a reduced muscle Treg compartment (Fig. 4*F*) vis-à-vis their control littermates.

Discussion

In murine skeletal muscle, a population of mSCs expressing IL-33 resides adjacent to peripheral nerve structures (7). Given the known role of IL-33 in promoting local expansion of muscle Tregs (7), these cells are well positioned to communicate with both the adaptive immune system and the peripheral nervous system. We have now demonstrated a strikingly close physical association between $IL\text{-}33^+$ MmSCs and both nerve bundles and small-fiber sensory neurons; established that MmSCs transcribe a number of genes encoding neuropeptides, neuropeptide receptors, and other nerve-related proteins; identified, in particular, MmSC subtypes that express both IL-33 and the CGRP receptor; and showed that up- or down-regulation of CGRP signaling increased or decreased, respectively, IL-33 production by MmSCs and eventually muscle Treg accumulation. These findings raise several points of interest.

Most studies of neural-immune cell interactions have focused on their direct, often bidirectional, crosstalk (18–22). Here, the finding that particular MmSC subtypes produce IL-33 points to a potentially underrecognized role of tissue stromal cells in orchestrating such conversations. Just as the importance of stromal cells in controlling the tumor microenvironment is increasingly recognized, their place in regulating neural-immune cell interactions would be consistent with a crucial role as conveyers of signals across systems.

Among the potential nervous-immune system interactions, a connection between peripheral sensory neurons and innate immune cells makes sense, given their shared responsibility for a rapid response to tissue damage. However, the role of neuropeptide signaling in coordinating the adaptive immune response has also long been recognized (23, 24). Our observation that systemic CGRP administration promoted local Treg expansion in uninjured muscle, possibly priming the tissue for an eventual anti-inflammatory response, is consistent with prior studies demonstrating the role of CGRP in suppressing activation of the adaptive immune system. CGRP directly inhibits T cell proliferation, as well as T helper (Th)1 IL-2 production (25, 26), inhibits dendritic cell migration (27), and promotes Th2 immunity (28). Muscle damage is accompanied by pain, a sensation driven by nociceptive neurons. It makes physiological sense that nociceptive neurons also act on MmSCs to drive Treg function. Within this context, signaling via IL-33–producing MmSCs may serve to more gradually and controllably transmit and augment early damage signals detected by the peripheral sensory nervous system into an eventual dampening of the adaptive immune response. In this regard, it is interesting that recent studies have highlighted a role for CGRP-mediated inhibition of the accumulation and function of type 2 innate lymphoid cells in the lung and small intestine (29–31). This effect is the opposite of that we observed for muscle Tregs, although the outcome, dampening of the inflammatory response, would be the same.

Several lines of evidence argue that the effect of CGRP on MmSCs is a direct one: they are physically associated with CGRP-inducing neurons, they are the major muscle cell type expressing both subunits of the CGRP receptor, and, as already evident at 4 h after CGRP injection, their IL-33 response is quite

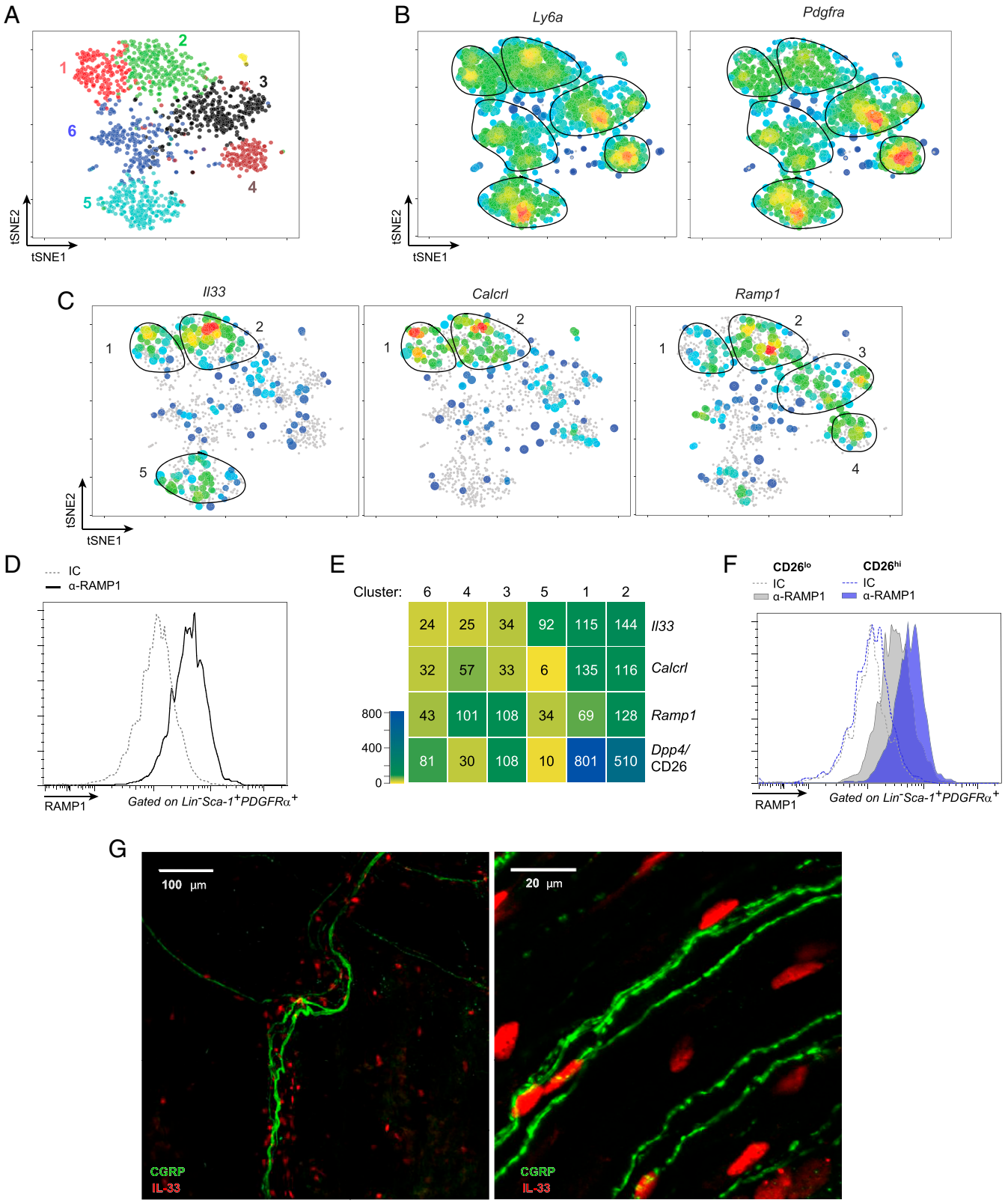

Fig. 3. IL-33–producing MmSCs express the CGRP neuropeptide receptor complex. (*A*–*G*) Analysis on uninjured hindlimb muscle. (*A*) Distinct clusters of MmSCs from single-cell RNA sequencing. (*B* and *C*) Heat map representation of gene expression by cluster for *Ly6a* (*B, Left*); *Pdgfra* (*B, Right*); *Il33* (*C, Left*); *Calcrl* (*C, Middle*); and *Ramp1* (*C, Right*). (*D*) Ramp1 mean fluorescence intensity distribution compared with isotype control (IC) from flow cytometry of MmSCs. (*E*) Average expression of *Il33*, *Calcrl*, *Ramp1*, and *Dpp4* (CD26) by cluster. (*F*) Ramp1 MFI distribution based on level of CD26 expression on MmSCs. (*G*) Immunofluorescence imaging of IL-33$^+$ cells and CGRP$^+$ nerve fibers.

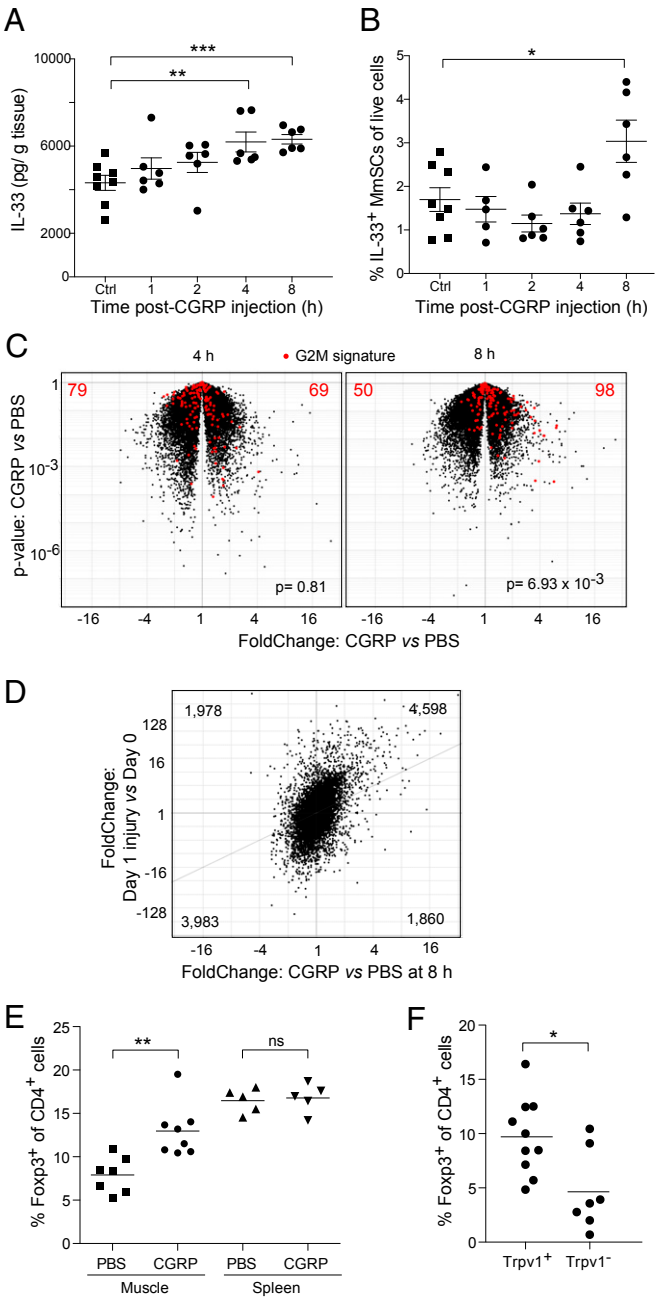

Fig. 4. CGRP affects IL-33 levels within skeletal muscle and results in Treg modulation. (*A–F*) Analysis on mice injected once i.p. with CGRP or PBS unless otherwise noted. (*A*) Muscle IL-33 levels as determined by ELISA. (*B*) IL-33$^+$ mSCs in muscle by flow cytometry. (*C*) Volcano plot comparisons of mSCs after CGRP vs. PBS injection. Quadruplicate samples. G2M signature highlighted in red with numbers indicating up-regulated and down-regulated genes. Not shown: Gal (4, 8 h; 174, 119 FC), Cxcl5 (8 h; 178 FC). (*D*) Fold-change by fold-change plot comparing effects of CGRP injection at 8 h and muscle CTX-injury. Numbers indicate genes per quadrant. Not shown: Gal (119, 2 FC), Cxcl5 (178, 3777 FC). (*E*) Flow cytometry of Tregs after CGRP injection (i.p. every 8 h, for 2 d). (*F*) Flow cytometry of Tregs in uninjured muscle of nociceptor-ablated mice (*Trpv1-Cre*$^{+/-}$*/Dta*$^{+/-}$; *Trpv1*$^-$) or littermate controls (*Trpv1-Cre*$^{-/-}$*/Dta*$^{+/-}$; *Trpv1*$^+$). All *P* values represent the unpaired *t* test, with **P* < 0.05; ***P* < 0.01; ****P* < 0.001.

rapid. Muscle Tregs can also respond directly to CGRP, in addition to IL-33, but they express lower levels of CGRP receptor transcripts and accumulate with delayed kinetics.

As demonstrated by scRNA-seq analysis, the MmSC compartment was quite heterogeneous. From the sorted CD45$^-$CD31$^-$Sca-1$^+$PDGFRα$^+$ population, only two of the six identified subtypes expressed both IL-33 and the two CGRP receptor subunits. It would be of interest to further investigate whether these subtypes have distinctive physical distributions within the muscle tissue before and after injury, and to follow their dynamics through muscle recovery from injury.

Nav1.8 is a voltage-gated ion channel that mediates action potential firing in nociceptive neurons, and humans with mutations in this ion channel show changes in pain sensitivity. Recent work has shown that Tregs can be potent regulators of pain in mouse models of sciatic nerve injury and experimental autoimmune neuritis (32, 33), as well as in experimental autoimmune encephalitis (34). Tregs could modulate pain through several molecular mechanisms. T cells express proenkephalin (Penk), which encodes endogenous opioid peptides that can potently suppress visceral pain (35). T cell-derived IL-10 also plays a critical role for resolution of chemotherapy-induced neuropathic pain (36), although this study indicated a role for CD8$^+$, rather than CD4$^+$, T cells. A connection between Nav1.8$^+$ neurons and their regulation of Tregs has not been previously described. It would be interesting if generation of pain after injury feeds back to induce more Tregs within muscles and other tissues, which in turn feeds back to silence pain. Pain might therefore be a way to trigger the body's inflammation-resolution mechanisms during wound healing that in turn also silence pain, which is one of the cardinal signs of inflammation itself.

Given that both are dispersed organ systems and both can respond rapidly to environmental challenges, interactions between the nervous and immune systems have long been studied (37–39). However, there has been a recent resurgence of interest in this area, with the advent of more sensitive and discriminating techniques in immunology, neurobiology, and genomics allowing for increasingly finer dissection of these interdependent networks and their physiologic relevance. Therapeutic applications are emerging, including evidence for vagal nerve stimulation in controlling chronic inflammatory disorders (40) and the recent approval of CGRP receptor antagonists and anti-CGRP antibodies for prevention of migraine headaches. Defining the role of tissue stromal cells in orchestrating the interplay between these networks will bring further insights into understanding the many disorders affecting peripheral nerves and tissue inflammation, such as immune-mediated neuropathies, chronic pain, and delayed wound healing.

Materials and Methods

Mice. The following mice were used: C57BL/6 (Jackson Laboratory), B6.*Nav1.8-Cre*$^{+/-}$*/TdTomato*$^{+/-}$ mice (B6.*Nav1.8/TdTomato* in the manuscript), nociceptor-ablated B6.*Trpv1-Cre*$^{+/-}$*/Dta*$^{+/-}$ mice and littermate controls B6.*Trpv1-Cre*$^{-/-}$*/Dta*$^{+/-}$, and B6.*Foxp3-IRES-GFP* mice obtained from V. Kuchroo (Brigham and Women's Hospital, Boston, MA).

Injections. Before muscle injury with Naja mossambica CTX, mice were anesthetized with i.p. injected ~200 μL (7 μL/g mouse weight) ketamine (10 mg/mL; Zoetis) and xylazine (2 mg/mL; Bimeda). CTX was injected into hindlimb muscles at 30 μL/muscle (0.03 mg/mL, Sigma), as previously described (13). CGRP (rat; R&D systems) was injected i.p. at 1.5 nmol in 200 μL PBS.

Histological Analyses. Mice were perfused with 4% PFA/PBS intracardially before muscles were harvested. Hindlimb muscle was postfixed with 4% PFA overnight and then permeabilized and blocked with 0.2% Triton X-100, 2% goat serum, and 2% BSA in PBS overnight at 4 °C. Tissue was sequentially stained with primary and secondary antibodies, placed in mounting media, and secured between a slide and coverslip by magnets.

Cell Isolation for Flow Cytometry. Mouse hindlimb muscles were minced and digested for 30 min at 37 °C in collagenase VIII (2 mg/mL; Invitrogen) and dispase (0.5 mg/mL; Invitrogen) for mSC isolation or in collagenase II (2 mg/mL; Invitrogen) and DNase I (150 mg/mL; Sigma) for muscle Treg isolation and then filtered through a 70 μM filter and washed twice before resuspension in staining medium. To separate the leukocyte fraction, the cells were

resuspended in 40% Percoll (GE Healthcare), underlaid with 80% Percoll, and spun at 25 min at 2,200 rpm with no brake. The interphase layer was then isolated and washed before resuspension in staining medium.

Flow Cytometry. Surface staining was performed for ~20 min on ice, and viability was assessed using Invitrogen LIVE/DEAD Fixable Near-IR Dead Cell Stain Kit as per manufacturer's instructions. Intracellular staining was performed using either the eBiosciences Intracellular Fixation & Permeabilization buffer set or the Biolegend True-Nuclear Transcription Factor buffer kit per manufacturer's protocol.

IL-33 ELISA. After muscles were harvested, a small piece of tissue (~40 to 50 mg) was removed from the center of the gastrocnemius and immediately frozen on dry ice. Protein extract was prepared as indicated in the *SI Appendix*. IL-33 ELISA (BioLegend) was performed using the manufacturer's protocol.

RNA-Sequencing. For population-level RNA-seq analysis, 1,000 double-sorted cells from each population were collected into 5 μL Buffer TCL (Qiagen) containing 1% beta-mercaptoethanol (Sigma) and sequenced by the Broad Technology Labs (41, 42). The single-cell dataset analysis was performed as previously described (43).

Pathway Analysis. KEGG Pathways Analysis was performed using Enrichr online tool (https://amp.pharm.mssm.edu/Enrichr/), using ±2 fold-change differentially expressed genes, with a P value <0.05 and an expression value ≥15.

Data Availability Statement. The data reported in this paper have been deposited in the Gene Expression Omnibus (GEO) database, https://www.ncbi.nlm.nih.gov/geo/ (accession no. GSE143428).

ACKNOWLEDGMENTS. We thank W. Kuswanto, M. Panduro, J. Cho, K. Hattori, A. Ortiz-Lopez, N. Asinovski, K. Seddu, A. Cook, F. Chen, L. Yang, G. Buruzula, C. Araneo, D. Ischiu Gutierrez, and F. Lopez for experimental assistance; and Dr. V. Kuchroo for providing mice. This work was funded by NIH grant R01 AR070334 and the JPB Foundation (to D.M.). Cell sorting was performed at the Harvard Stem Cell Institute/Joslin Diabetes Center Flow Cytometry Core (NIH P30DK036836 and S10OR021740), and at the Harvard Medical School Immunology Flow Cytometry Facility; InDrops was done at the HMS Single Cell Core. K.W. was supported by an HHMI Medical Research Fellowship, O.K.Y. by NIH Training Grant T32GM007753, R.G.S. by American Diabetes Association Postdoctoral Fellowship 1-17-PMF-005, X.C. by the Evergrande Center for Immunologic Diseases, and D.Z. by a PhD fellowship from Boehringer Ingelheim Fonds.

1. S. L. Foster, C. R. Seehus, C. J. Woolf, S. Talbot, Sense and immunity: Context-dependent neuro-immune interplay. *Front. Immunol.* **8**, 1463 (2017).
2. S. Talbot *et al.*, Silencing nociceptor neurons reduces allergic airway inflammation. *Neuron* **87**, 341–354 (2015).
3. L. Riol-Blanco *et al.*, Nociceptive sensory neurons drive interleukin-23-mediated psoriasiform skin inflammation. *Nature* **510**, 157–161 (2014).
4. P. Baral *et al.*, Nociceptor sensory neurons suppress neutrophil and γδ T cell responses in bacterial lung infections and lethal pneumonia. *Nat. Med.* **24**, 417–426 (2018).
5. S. W. Kashem *et al.*, Nociceptive sensory fibers drive interleukin-23 production from CD301b$^+$ dermal dendritic cells and drive protective cutaneous immunity. *Immunity* **43**, 515–526 (2015).
6. M. A. Engel *et al.*, TRPA1 and substance P mediate colitis in mice. *Gastroenterology* **141**, 1346–1358 (2011).
7. W. Kuswanto *et al.*, Poor repair of skeletal muscle in aging mice reflects a defect in local, interleukin-33-dependent accumulation of regulatory T cells. *Immunity* **44**, 355–367 (2016).
8. C. Cayrol, J. P. Girard, Interleukin-33 (IL-33): A nuclear cytokine from the IL-1 family. *Immunol. Rev.* **281**, 154–168 (2018).
9. C. Schiering *et al.*, The alarmin IL-33 promotes regulatory T-cell function in the intestine. *Nature* **513**, 564–568 (2014).
10. A. Vasanthakumar *et al.*, The transcriptional regulators IRF4, BATF and IL-33 orchestrate development and maintenance of adipose tissue-resident regulatory T cells. *Nat. Immunol.* **16**, 276–285 (2015).
11. D. Kolodin *et al.*, Antigen- and cytokine-driven accumulation of regulatory T cells in visceral adipose tissue of lean mice. *Cell Metab.* **21**, 543–557 (2015).
12. J. M. Han *et al.*, IL-33 reverses an obesity-induced deficit in visceral adipose tissue ST2$^+$ T regulatory cells and ameliorates adipose tissue inflammation and insulin resistance. *J. Immunol.* **194**, 4777–4783 (2015).
13. D. Burzyn *et al.*, A special population of regulatory T cells potentiates muscle repair. *Cell* **155**, 1282–1295 (2013).
14. A. W. Joe *et al.*, Muscle injury activates resident fibro/adipogenic progenitors that facilitate myogenesis. *Nat. Cell Biol.* **12**, 153–163 (2010).
15. J. E. Heredia *et al.*, Type 2 innate signals stimulate fibro/adipogenic progenitors to facilitate muscle regeneration. *Cell* **153**, 376–388 (2013).
16. F. A. Pinho-Ribeiro, W. A. Verri, Jr, I. M. Chiu, Nociceptor sensory neuron-immune interactions in pain and inflammation. *Trends Immunol.* **38**, 5–19 (2017).
17. S. K. Mishra, S. M. Tisel, P. Orestes, S. K. Bhangoo, M. A. Hoon, TRPV1-lineage neurons are required for thermal sensation. *EMBO J.* **30**, 582–593 (2011).
18. J. Ordovas-Montanes *et al.*, The regulation of immunological processes by peripheral neurons in homeostasis and disease. *Trends Immunol.* **36**, 578–604 (2015).
19. C. S. N. Klose *et al.*, The neuropeptide neuromedin U stimulates innate lymphoid cells and type 2 inflammation. *Nature* **549**, 282–286 (2017).
20. V. Cardoso *et al.*, Neuronal regulation of type 2 innate lymphoid cells via neuromedin U. *Nature* **549**, 277–281 (2017).
21. A. Wallrapp *et al.*, The neuropeptide NMU amplifies ILC2-driven allergic lung inflammation. *Nature* **549**, 351–356 (2017).
22. N. Yissachar *et al.*, An intestinal organ culture system uncovers a role for the nervous system in microbe-immune crosstalk. *Cell* **168**, 1135–1148.e12 (2017).
23. D. G. Payan, J. D. Levine, E. J. Goetzl, Modulation of immunity and hypersensitivity by sensory neuropeptides. *J. Immunol.* **132**, 1601–1604 (1984).
24. M. Levite, Neuropeptides, by direct interaction with T cells, induce cytokine secretion and break the commitment to a distinct T helper phenotype. *Proc. Natl. Acad. Sci. U.S.A.* **95**, 12544–12549 (1998).
25. Y. Umeda, M. Takamiya, H. Yoshizaki, M. Arisawa, Inhibition of mitogen-stimulated T lymphocyte proliferation by calcitonin gene-related peptide. *Biochem. Biophys. Res. Commun.* **154**, 227–235 (1988).
26. F. Wang, I. Millet, K. Bottomly, A. Vignery, Calcitonin gene-related peptide inhibits interleukin 2 production by murine T lymphocytes. *J. Biol. Chem.* **267**, 21052–21057 (1992).
27. S. Dunzendorfer, A. Kaser, C. Meierhofer, H. Tilg, C. J. Wiedermann, Cutting edge: Peripheral neuropeptides attract immature and arrest mature blood-derived dendritic cells. *J. Immunol.* **166**, 2167–2172 (2001).
28. N. Mikami *et al.*, Calcitonin gene-related peptide is an important regulator of cutaneous immunity: Effect on dendritic cell and T cell functions. *J. Immunol.* **186**, 6886–6893 (2011).
29. A. Wallrapp *et al.*, Calcitonin gene-related peptide negatively regulates alarmin-driven type 2 innate lymphoid cell responses. *Immunity* **51**, 709–723.e6 (2019).
30. H. Nagashima *et al.*, Neuropeptide CGRP limits group 2 innate lymphoid cell responses and constrains type 2 inflammation. *Immunity* **51**, 682–695.e6 (2019).
31. H. Xu *et al.*, Transcriptional atlas of intestinal immune cells reveals that neuropeptide α-CGRP modulates group 2 innate lymphoid cell responses. *Immunity* **51**, 696–708.e9 (2019).
32. P. J. Austin, C. F. Kim, C. J. Perera, G. Moalem-Taylor, Regulatory T cells attenuate neuropathic pain following peripheral nerve injury and experimental autoimmune neuritis. *Pain* **153**, 1916–1931 (2012).
33. J. G. Lees, S. S. Duffy, C. J. Perera, G. Moalem-Taylor, Depletion of Foxp3$^+$ regulatory T cells increases severity of mechanical allodynia and significantly alters systemic cytokine levels following peripheral nerve injury. *Cytokine* **71**, 207–214 (2015).
34. S. S. Duffy *et al.*, Regulatory T cells and their derived cytokine, interleukin-35, reduce pain in experimental autoimmune encephalomyelitis. *J. Neurosci.* **39**, 2326–2346 (2019).
35. L. Basso *et al.*, Endogenous control of inflammatory visceral pain by T cell-derived opioids in IL-10-deficient mice. *Neurogastroenterol. Motil.* **32**, e13743 (2019).
36. K. Krukowski *et al.*, CD8$^+$ T cells and endogenous IL-10 are required for resolution of chemotherapy-induced neuropathic pain. *J. Neurosci.* **36**, 11074–11083 (2016).
37. E. Weihe *et al.*, Molecular anatomy of the neuro-immune connection. *Int. J. Neurosci.* **59**, 1–23 (1991).
38. D. E. James, F. P. Nijkamp, Neuro-immune interactions in the lung. *Clin. Exp. Allergy* **29**, 1309–1319 (1999).
39. H. Schneider *et al.*, A neuromodulatory role of interleukin-1beta in the hippocampus. *Proc. Natl. Acad. Sci. U.S.A.* **95**, 7778–7783 (1998).
40. R. L. Johnson, C. G. Wilson, A review of vagus nerve stimulation as a therapeutic intervention. *J. Inflamm. Res.* **11**, 203–213 (2018).
41. S. Picelli *et al.*, Full-length RNA-seq from single cells using Smart-seq2. *Nat. Protoc.* **9**, 171–181 (2014).
42. C. Trapnell *et al.*, Differential gene and transcript expression analysis of RNA-seq experiments with TopHat and cufflinks. *Nat. Protoc.* **7**, 562–578 (2012).
43. R. G. Spallanzani *et al.*, Distinct immunocyte-promoting and adipocyte-generating stromal components coordinate adipose tissue immune and metabolic tenors. *Sci. Immunol.* **4**, eaaw3658 (2019).

SUPPPORTING INFORMATION

METHODS

Mice

C57BL/6 mice (B6, Jax #000664) were purchased from the Jackson Laboratory (Jax) and used at the specified ages. Nav1.8-Cre mice were initially generated by Dr. John Wood (University College London, United Kingdom) and were bred with B6.Cg-*Gt(ROSA)26Sor*$^{tm14(CAG-tdTomato)Hze}$/J mice (ai14, Jax #007914) to generate B6.Nav1.8-Cre$^{+/-}$/TdTomato$^{+/-}$ mice (B6.*Nav1.8/TdTomato* in the manuscript). B6.129-*Trpv1*$^{tm1(cre)Bbm}$/J heterozygous (+/−) mice (TRPV1^{Cre}, Jax #017769) were crossed with B6.129P2-*Gt(ROSA)26Sor*$^{tm1(DTA)Lky}$/J homozygous (+/+) mice (ROSA-DTA, Jax #009669) to generate nociceptor-ablated B6.*Trpv1-Cre*$^{+/-}$*/Dta*$^{+/-}$ mice and littermate controls B6.*Trpv1-Cre*$^{-/-}$*/Dta*$^{+/-}$. B6.*Foxp3-IRES-GFP* (Foxp3^{GFP}) mice were obtained from V. Kuchroo, Brigham and Women's Hospital, Boston. Experiments were conducted under protocols approved by Harvard Medical School's Institutional Animal Care and Use Committee and housed in specific-pathogen-free facilities at Harvard Medical School.

Injections

Before muscle injury with *Naja mossambica* cardiotoxin (CTX), mice were anesthetized with an intraperitoneal (i.p.) injection of ~200 μL (7 μL/g mouse weight) of ketamine (10 mg/mL; Zoetis) and xylazine (2 mg/mL; Bimeda). CTX was injected into hindlimb muscles (tibialis anterior, gastrocnemius, and quadriceps) at 30 μL/muscle (0.03 mg/mL, Sigma) as previously described (1). CGRP (rat; R&D systems) was injected i.p. at 1.5 nmol in 200 μL of PBS.

Histological analyses

To prepare samples for whole-mount staining, mice were perfused with 4% PFA/PBS intracardially before muscles were harvested. Hindlimb muscle was post-fixed with 4% PFA overnight, then permeabilized and blocked with 0.2% Triton X-100, 2% goat serum, and 2% BSA in PBS overnight at 4°C. Whole mount muscle was stained with primary antibody in 0.2% Triton X-100/2% BSA in PBS for 1 day at 4°C and washed with PBS 3 times over the course of the next day. The whole-mount was then stained with secondary antibody in 0.2% Triton X-100/2% BSA in PBS overnight, and washed 3 times with PBS over the course of the next day. The sample was soaked in mounting media and secured in place between a slide and cover slip by magnets. The following antibodies were used for staining: goat polyclonal anti-mouse IL-33 (1:50, R&D), rabbit anti-mouse S100 (1:100, Abcam), rabbit anti-mouse β3-tubulin (1:50, Abcam), mouse anti-CGRP (1:50, Abcam), donkey anti-goat IgG (1:100, Jackson), and donkey anti-rabbit IgG (1:100, Jackson). Images were acquired on the Olympus Fluoview confocal microscope.

Cell isolation for flow cytometry

For isolation of mSCs, mouse hindlimb muscles were excised, minced, and digested in collagenase VIII (2 mg/mL, Invitrogen) and dispase (0.5 mg/mL, Invitrogen) for 30 minutes at 37°C, then filtered through a 70 μM filter and washed twice before resuspension in staining medium.

For isolation of muscle Tregs, hindlimb muscles were excised, minced, and digested in collagenase II (2 mg/mL, Invitrogen) and DNase I (150 mg/mL, Sigma) for 30 minutes at 37°C, then filtered through a 70 μM filter and washed. To separate the leukocyte fraction, the cells were resuspended in 40% Percoll (GE Healthcare), underlaid with 80% Percoll, and spun at 25

min at 2200 rpm with no brake. The interphase layer was then isolated and washed before resuspension in staining medium.

Flow cytometry

The following antibodies were used for flow cytometry analysis of mSCs: Biolegend anti-CD45 (30-F11), anti-CD31 (390), anti-PDGFRα (APA5), anti-Sca-1 (D7), and anti-podoplanin (8.1.1); R&D goat anti-mouse IL-33 (AF3626); Jackson Labs donkey anti-goat Cy3; Alomone Labs anti-Ramp1 (ARR-021); and Invitrogen LIVE/DEAD^{TM} Fixable Near-IR Dead Cell Stain Kit. Intracellular staining was performed using the Biolegend True-Nuclear Transcription Factor buffer kit per manufacturer's protocol.

The following antibodies were used for analysis of Tregs: Biolegend anti-CD45 (30-F11), anti-TCRb (H57-597), anti-CD4 (GK1.5), anti-CD8 (53-6.7) and anti-CD25 (PC61); and eBioscience anti-Foxp3 (FJK-16s). Intracellular staining was performed using the eBiosciences Intracellular Fixation & Permeabilization buffer set per manufacturer's protocol.

Data were acquired with BD Biosciences LSR II and analyzed using FlowJo software.

IL-33 ELISA

After muscles were harvested, a small piece of tissue (~40-50 mg) was removed from the center of the gastrocnemius and immediately frozen on dry ice. Samples were stored at -80°C prior to performing the ELISA. To prepare samples for ELISA, tissues were thawed and 500 μL of RIPA buffer (GeneTex) mixed with cOmplete protease inhibitors (Roche) was added to each sample. Tissue was then minced with scissors and further processed with a hand-held homogenizer (VWR). Samples incubated at 4°C on a rotator for 2 hours and then were centrifuged down for 20 minutes at 13,000 rpm. Supernatants were transferred to a new tube and the Bradford assay (ThermoFisher Scientific) was used to determine total protein

concentrations. Samples were diluted to 5 mg/mL and 100 μL per sample was used for the assay. IL-33 ELISA (BioLegend) was performed using the manufacturer's protocol.

RNA-sequencing

For population-level RNA-seq analysis, cell suspensions were prepared and stained with Abs against CD45, CD31, Sca-1, and PDGFRα, utilizing DAPI to identify viable cells. Samples were double-sorted and one thousand cells from each population were collected into 5 μl Buffer TCL (Qiagen) containing 1% beta-mercaptoethanol (Sigma). Smart-Seq2 libraries were prepared by the Broad Technology Labs, and were sequenced using the Broad Genomics Platform (2). Briefly, total RNA was captured and purified on RNAClean XP beads (Beckman Coulter). Polyadenylated mRNA was then selected using an anchored oligo(dT) primer and converted to cDNA via reverse transcription. First-strand cDNA was subjected to limited PCR amplification followed by transposon-based fragmentation using the Nextera XT DNA Library Preparation Kit (Illumina). Samples were then PCR-amplified using barcoded primers such that each sample carried a specific combination of Illumina P5 and P7 barcodes, and were pooled prior to sequencing. Sequencing was performed on an Illumina NextSeq500 using 2 x 25bp reads. Transcripts were quantified by the Broad Technology Labs computational pipeline using Cuffquant version 2.2.1 (3).

The single-cell dataset is from GSE127005 and the analysis was performed as previously described (4).

Pathway analysis

KEGG Pathways Analysis was performed using Enrichr online tool (https://amp.pharm.mssm.edu/Enrichr/), using ± 2 fold-change differentially expressed genes, with a P-value < 0.05 and an expression value ≥ 15 (5, 6).

Statistical analyses

Data is displayed as mean + SD in Figure 2 and S1 or mean +/- SEM in Figure 4 and S2. Analysis in Figure 1 was performed in R and the P-value was determined by the Kolmogorov-Smirnov test. Otherwise, analyses were done using GraphPad Prism version 8 and P-values calculated by the unpaired t-test, with *<0.05; **<0.01; ***<0.001.

SI REFERENCES

1. Burzyn D, et al. (2013) A special population of regulatory T cells potentiates muscle repair. *Cell* 155(6): 1282-1295.
2. Picelli S, et al. (2014) Full-length RNA-seq from single cells using Smart-seq2. *Nat Protoc.* 9(1): 171-181.
3. Trapnell C, et al. (2012) Differential gene and transcript expression analysis of RNA-seq experiments with TopHat and Cufflinks. *Nat Protoc.* 7(3): 562-578.
4. Spallanzani RG, et al. (2019) Distinct immunocyte-promoting and adipocyte-generating stromal components coordinate adipose tissue immune and metabolic tenors. *Sci Immunol* 4(35).
5. Chen EY, et al. (2013) Enrichr: interactive and collaborative HTML5 gene list enrichment analysis tool. *BMC. Bioinformatics.* 14 128.
6. Kuleshov MV, et al. (2016) Enrichr: a comprehensive gene set enrichment analysis web server 2016 update. *Nucleic Acids Res.* 44(W1): W90-W97.

SI FIGURE LEGENDS

Fig. S1. Lymph node mSCs express genes involved in neural signaling. (*A-C*) RNA-seq analysis of mSCs isolated from inguinal, axillary, brachial and cervical lymph nodes. Triplicate samples. Average expression of select genes encoding neuropeptides (*A*), neuropeptide receptors (*B*) and other nerve-related genes involved in neurotrophic signaling, neuromodulation and axon guidance (*C*).

Figure S2: Flow cytometry of MmSCs during CGRP vs PBS time course in Figure 4b. (*A*) Gating scheme. (*B*) Percentage of viable MmSCs. (*C*) Contribution of different cellular compartments to IL-33 production in the muscle. Double negative (DN) indicates $CD31^{-}CD45^{-}$ $Sca\text{-}1^{-}PDGFR\alpha^{-}$. Podoplanin (PDPN) is an additional surface marker of MmSCs.

FIGURE S1

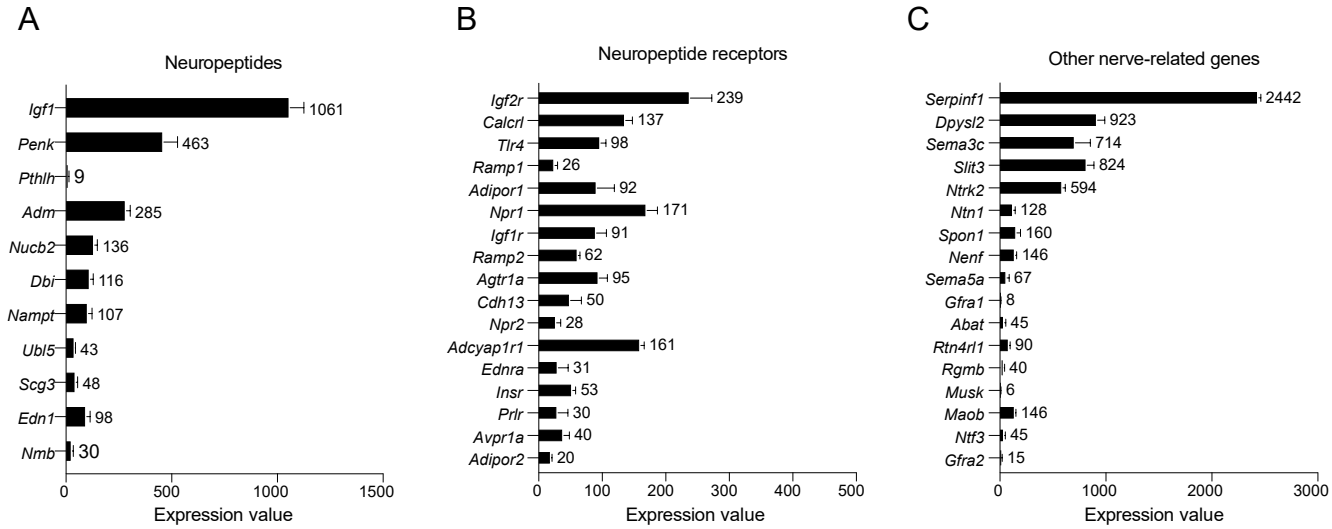
A
Neuropeptides
Igf1
Penk
Pthlh
Adm
Nucb2
Dbi
Nampt
Ubl5
Scg3
Edn1
Nmb
1061
463
9
285
136
116
107
43
48
98
30
0
500
1000
1500
Expression value
B
Neuropeptide receptors
Igf2r
Calcrl
Tlr4
Ramp1
Adipor1
Npr1
Igf1r
Ramp2
Agtr1a
Cdh13
Npr2
Adcyap1r1
Ednra
Insr
Prlr
Avpr1a
Adipor2
239
137
98
26
92
171
91
62
95
50
28
161
31
53
30
40
20
0
100
200
300
400
500
Expression value
C
Other nerve-related genes
Serpinf1
Dpysl2
Sema3c
Slit3
Ntrk2
Ntn1
Spon1
Nenf
Sema5a
Gfra1
Abat
Rtn4rl1
Rgmb
Musk
Maob
Ntf3
Gfra2
2442
923
714
824
594
128
160
146
67
8
45
90
40
6
146
45
15
0
1000
2000
3000
Expression value

FIGURE S2

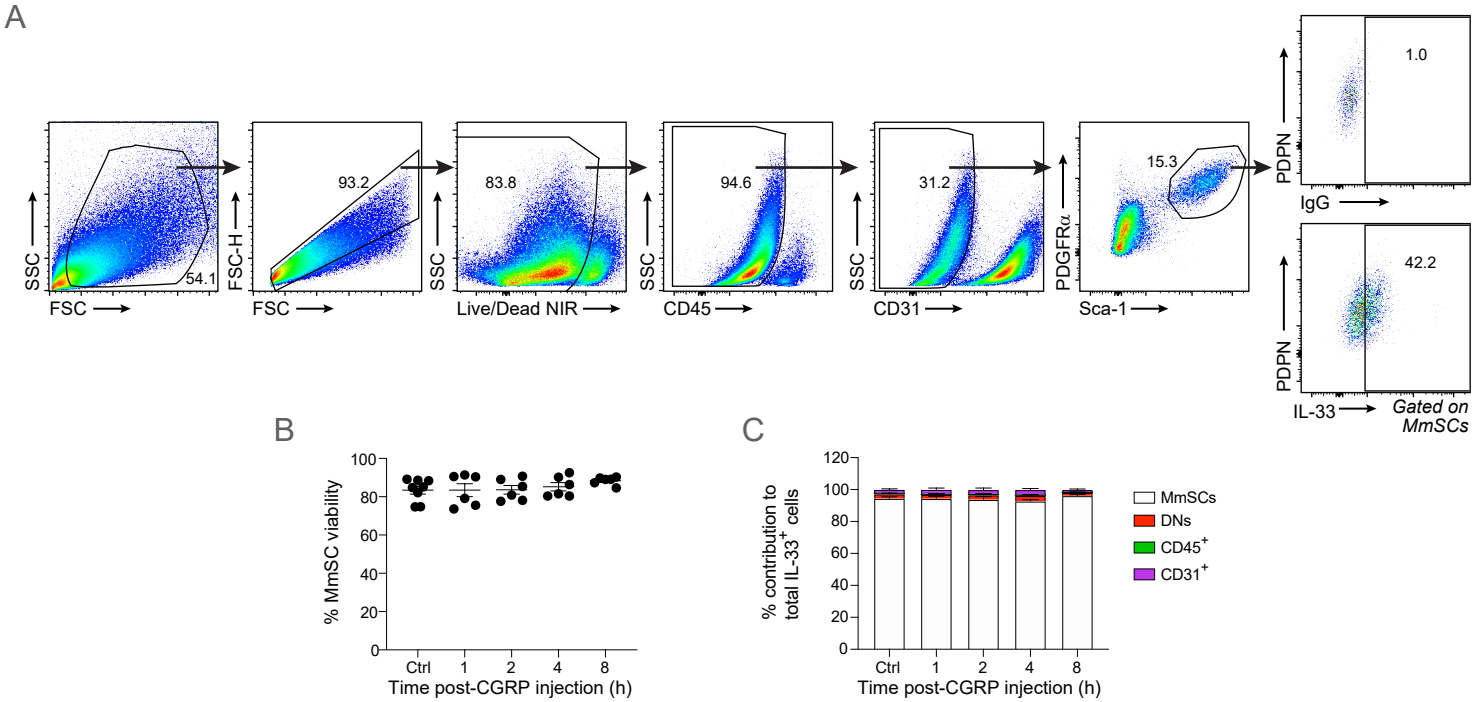
A
SSC
FSC
54.1
FSC-H
FSC
93.2
SSC
Live/Dead NIR
83.8
SSC
CD45
94.6
SSC
CD31
31.2
PDGFRα
Sca-1
15.3
PDPN
IgG
1.0
PDPN
IL-33
42.2
Gated on MmSCs
B
% MmSC viability
100
80
60
40
20
0
Ctrl
1
2
4
8
Time post-CGRP injection (h)
C
% contribution to total IL-33+ cells
120
100
80
60
40
20
0
Ctrl
1
2
4
8
Time post-CGRP injection (h)
MmSCs
DNs
CD45+
CD31+

SI TABLE LEGENDS

Table S1: Average expression of *Calcrl* and *Ramp* gene family members within various cellular compartments in the muscle. RNA-seq of $CD45^+$, $CD31^+$, mSCs, and muscle satellite cells (MuSCs) isolated from uninjured hindlimb muscle. Triplicate samples.

Table S2: Pathway analysis on CGRP-induced transcriptomic changes. Top 8 significantly enriched KEGG pathways corresponding to CGRP vs PBS MmSCs at 4 and 8 hours post-CGRP injection. % Overlap represents the fraction of enriched genes out of the total genes within each pathway.

Table S1

Gene	CD31$^+$	CD45$^+$	MmSC	MuSC
Calcrl	573.5	90.8	429.6	49.2
Ramp1	9.5	437.8	765.7	1.7
Ramp2	2804.5	5.0	601.5	286.3
Ramp3	129.7	4.0	1.4	1.0

Table S2

CGRP vs PBS at 4 h Up Signature

Term	% Overlap	P-value	Combined Score	Genes
Type II diabetes mellitus	8.3	$8.7x10^{-4}$	66.0	*Socs3;Socs1;Cacna1C;Hk2*
Amino sugar and nucleotide sugar metabolism	8.2	$9.4x10^{-4}$	63.9	*Ugdh;Gfpt2;Uap1;Hk2*
Mineral absorption	6.8	$7.0x10^{-3}$	38.0	*Vdr;Mt2;Mt1*
Complement and coagulation cascades	4.5	$7.9x10^{-3}$	24.7	*Thbd;Procr;Bdkrb2;Bdkrb1*
Chemokine signaling pathway	3.0	$8.5x10^{-3}$	16.3	*Cx3Cr1;Gng4;Ccl2;Rac1;Cxcl13;Jak3*
Pathways in cancer	2.1	$8.5x10^{-3}$	11.0	*Txnrd3;Gng4;Pim1;Slc2A1;Bdkrb2;Bdkrb1;Rac1;Ptgs2;Jak3;Runx1;Fgf10*
Arginine and proline metabolism	6.0	$1.0x10^{-2}$	31.0	*Odc1;Prodh;Srm*
AGE-RAGE signaling pathway in diabetic complications	4.0	$1.2x10^{-2}$	19.4	*Thbd;Pim1;Ccl2;Rac1*

CGRP vs PBS at 4 h Down Signature

Term	% Overlap	P-value	Combined Score	Genes
Axon guidance	4.4	$5.3x10^{-4}$	32.8	*Ephb6;Epha4;Unc5B;Sema3D;Wnt5A;Pak3;Myl9;Epha3*
Metabolism of xenobiotics by cytochrome P450	7.6	$5.6x10^{-4}$	55.5	*Adh1;Gsta4;Mgst3;Gstt1;Cyp2F2*
Vascular smooth muscle contraction	4.3	$3.1x10^{-3}$	24.2	*Itpr3;Mrvi1;Adm;Myl9;Adra1A;Mylk*
Cushing syndrome	3.8	$5.8x10^{-3}$	19.0	*Cdk6;Wnt5A;E2F1;Itpr3;Ldlr;Cacna1G*
Wnt signaling pathway	3.8	$6.0x10^{-3}$	18.8	*Daam2;Wif1;Wnt5A;Rspo2;Rspo3;Nkd2*
Hepatocellular carcinoma	3.5	$8.2x10^{-3}$	16.5	*Cdk6;Gsta4;Mgst3;Wnt5A;E2F1;Gstt1*
cGMP-PKG signaling pathway	3.5	$8.5x10^{-3}$	16.3	*Itpr3;Mrvi1;Adrb2;Myl9;Adra1A;Mylk*
Neuroactive ligand-receptor interaction	2.6	$9.6x10^{-3}$	11.8	*Gabrr2;P2Ry6;Grm8;Npy1R;Aplnr;Adm;Adrb2;Prlr;Adra1A*

CGRP vs PBS at 8 h Up Signature

Term	% Overlap	P-value	Combined Score	Genes
Chemokine signaling pathway	3.6	$4.9x10^{-5}$	72.7	*Ccl7;Gng4;Ccl2;Cxcl13;Cxcl14;Cxcl5;Pik3R5*
Cytokine-cytokine receptor interaction	2.7	$8.8x10^{-5}$	52.7	*Il1rl1;Tnfrsf12A;Ccl7;Il1R2;Ccl2;Cxcl13;Cxcl14;Cxcl5*
ECM-receptor interaction	4.8	$7.1x10^{-4}$	72.0	*Sv2C;Tnc;Sdc1;Thbs1*
IL-17 signaling pathway	4.4	$1.0x10^{-3}$	62.5	*Fosl1;Ccl7;Ccl2;Cxcl5*
Malaria	6.1	$1.7x10^{-3}$	80.3	*Ccl2;Sdc1;Thbs1*
Pyrimidine metabolism	5.2	$2.8x10^{-3}$	62.6	*Dctd;Uck2;Ctps*
Proteoglycans in cancer	2.5	$3.1x10^{-3}$	29.3	*Plaur;Sdc1;Wnt2;Thbs1;Hbegf*
Synaptic vesicle cycle	3.9	$6.2x10^{-3}$	40.8	*Slc6A13;Slc6A12;Slc6A2*

CGRP vs PBS at 8 h Down Signature

Term	% Overlap	P-value	Combined Score	Genes
Vascular smooth muscle contraction	3.6	$9.7x10^{-4}$	45.8	*Gucy1A2;Edn1;Avpr1A;Myl9;Adra1A*
Axon guidance	2.8	$2.9x10^{-3}$	30.0	*Sema5A;Robo2;Camk2B;Epha4;Myl9*
Drug metabolism	3.5	$3.4x10^{-3}$	36.9	*Gsta4;Fmo1;Fmo2;Cyp2E1*
Metabolism of xenobiotics by cytochrome P450	4.5	$5.4x10^{-3}$	43.8	*Gsta4;Cyp2E1;Cyp2F2*
Adrenergic signaling in cardiomyocytes	2.7	$8.5x10^{-3}$	23.9	*Camk2B;Cacnb4;Bcl2;Adra1A*
Oxytocin signaling pathway	2.6	$9.7x10^{-3}$	22.3	*Camk2B;Gucy1A2;Cacnb4;Myl9*
Neuroactive ligand-receptor interaction	1.7	$1.1x10^{-2}$	14.2	*Gabrr2;Edn1;Grm8;Aplnr;Avpr1A;Adra1A*
cGMP-PKG signaling pathway	2.3	$1.4x10^{-2}$	18.3	*Gucy1A2;Irs1;Myl9;Adra1A*